

1      **Rapid Communication: Middle Pleistocene Transition as a Phenomenon of**  
2      **Orbitally Enabled Sensitivity to Initial Values**

4      Mikhail Y. Verbitsky<sup>1,2</sup> and Anne Willem Omta<sup>3</sup>

5      <sup>1</sup>Gen5 Group, LLC, Newton, MA, USA

6      <sup>2</sup>UCLouvain, Earth and Life Institute, Louvain-la-Neuve, Belgium

7      <sup>3</sup>Department of Earth, Environmental, and Planetary Sciences, Case Western Reserve University, Cleveland, OH, USA

8      Correspondence: Mikhail Verbitsky (verbitskys@gmail.com)

10     **Abstract.** The Middle Pleistocene Transition (MPT), i.e., the “fast” transition from ~41- to ~100-kyr  
11     rhythmicity that occurred about 1 Myr ago, remains one of the most intriguing phenomena of the past  
12     climate. The cause of this period shift is generally thought to be a change within the Earth System, since  
13     the orbital insolation forcing does not change its pattern through the MPT. Using a dynamical model  
14     rooted in ocean chemistry, we advance several novel concepts here: (i) the MPT could be a dominant-  
15     period relaxation process that may be dependent on the initial state of the system, (ii) this sensitivity to  
16     the initial state is enabled by the orbital forcing, (iii) depending on the amplitude of the orbital forcing and  
17     initial values, the MPT could have been not just of the 40 – 80 kyr type, as we observe in the available  
18     data, but also of a 20 – 40, 40 – 120, or even 80 – 40 kyr type, (iv) when the orbital forcing of the global  
19     glaciation-climate model is accompanied by the alkalinity ( $\text{CO}_2$ ) forcing containing a dominant-period  
20     shift from 41 kyr to 80 kyr, this ice-climate system produces a 40-to-100 kyr glacial rhythmicity transition  
21     resembling the MPT LR04 data, and (v) when the glaciation-climate model is forced by an alkalinity  
22     ( $\text{CO}_2$ ) forcing containing a periodicity transition from 20 kyr to 42 kyr, a non-linear interplay of the  
23     orbital forcing and of ~40-kyr periods of the alkalinity forcing may produce glaciation periods of ~100  
24     kyr that are also consistent with the LR04 data.

25     **1. Introduction**

28     Around 1 Myr ago, the dominant period of the glacial-interglacial cycles shifted from ~41 to ~100  
29     kyr. The disambiguation of this change in glacial rhythmicity, i.e., the Middle Pleistocene Transition, or  
30     MPT hereafter, has been a challenge for the scientific community throughout the last few decades (e.g.,  
31     Saltzman and Verbitsky, 1993; Clark and Pollard, 1998; Tziperman et al., 2006; Peacock et al., 2006; Abe-  
32     Ouchi et al., 2013; Crucifix, 2013; Mitsui and Aihara, 2014; Paillard, 2015; Ashwin and Ditlevsen, 2015;  
33     Verbitsky et al., 2018; Willeit et al., 2019; Riechers et al., 2022; Shackleton et al., 2023; Carrillo et al.,  
34     2025; Scherrenberg et al., 2025; Pérez-Montero et al., 2025). Since the orbital insolation forcing does not  
35     change its pattern through the MPT, several proposed hypotheses included slow changes in governing  
36     parameters *internal to the Earth System*. These may define intensities of positive (e.g., variations in  
37     carbon dioxide concentration, Saltzman and Verbitsky, 1993) or negative (e.g., regolith erosion, Clark  
38     and Pollard, 1998) system feedbacks or a combination of positive and negative feedbacks (e.g., the  
39     interplay of ice-sheet vertical temperature advection and the geothermal heat flux, Verbitsky and Crucifix,  
40     2021). The importance of the orbital forcing in generating the pre-MPT ~41 kyr cycles and post-MPT  
41     ~100 kyr cycles has widely been acknowledged. In particular, it has been suggested that orbital periods  
42     either directly drive these cycles (Raymo et al., 2006; Bintanja and Van de Wal, 2008; Tzedakis et al.,  
43     2017) or synchronize auto-oscillations of the Earth’s climate (Saltzman and Verbitsky, 1993; Tziperman  
44     et al., 2006; Rial et al., 2013; Nyman and Ditlevsen, 2019; Shackleton et al., 2023). However, the orbital  
45     forcing has not been considered to play a role in the origin of the MPT.

46     Recently, it has been proposed (Ma et al., 2024) that the amplitude of the orbital forcing may  
47     experience a change on a million-year timescale and this may have its effect on the MPT. Verbitsky and  
48     Volobuev (2024) suggested that the orbital forcing may play an even bigger role and can also change the  
49     dynamical properties of the Earth’s climate system. For example, it may change the timescale of the

50 vertical advection of mass and temperature in ice sheets and make their dynamics sensitive to initial  
51 values. Is ice physics unique in this sense? To answer this question, in this paper we will consider the  
52 calcifier-alkalinity (C-A) model that describes entirely different physics, focusing on the interactions  
53 between a population of calcifying organisms and ocean alkalinity (Omta et al., 2013). Previously, it has  
54 been shown that:

55 (a) The C-A system relaxes slowly to its asymptotic state, i.e., it has a long memory of its initial  
56 conditions (Omta et al., 2013);

57 (b) The asymptotic state of the orbitally forced C-A system depends on its initial conditions (Omta et  
58 al., 2016).

59 We will demonstrate here that the relaxation of the dominant period of the orbitally forced C-A  
60 system from its initial value to the asymptotic value can include a sharp transition similar to the MPT. We  
61 will also perform a scaling analysis of the C-A model and demonstrate that the asymptotic dominant  
62 periods are defined by a conglomerate similarity parameter combining the amplitude of the orbital forcing  
63 and the initial values. In other words, *the orbital forcing enables the dominant-period sensitivity to initial*  
64 *values*. We will also prove that what we call an MPT-like event in terms of the alkalinity periodicity can  
65 be translated into an MPT event in terms of the glacial rhythmicity.

## 66 2. Ocean calcifier-alkalinity model

67 The C-A model was first formulated by Omta et al. (2013) and focuses on the throughput of alkalinity  
68 through the World's oceans. The alkalinity is a measure for the buffering capacity of seawater that  
69 controls its capacity for carbon storage through the carbonate equilibrium (Broecker and Peng, 1982;  
70 Zeebe and Wolf-Gladrow, 2001; Williams and Follows, 2011). Alkalinity is continuously transported into  
71 the oceans as a consequence of rock weathering on the continents. When alkalinity is added to the ocean,  
72 the solubility of  $\text{CO}_2$  increases leading to an uptake of carbon from the atmosphere into the ocean.  
73 Removal of alkalinity from the water (through incorporation of calcium carbonate into the shells of  
74 calcifying organisms and subsequent sedimentation) leads to a lower  $\text{CO}_2$  solubility and thus outgassing  
75 of carbon from the ocean into the atmosphere. The C-A model assumes that alkalinity  $A$  (mM eq) enters  
76 the ocean at a constant rate  $I_0$  (mM eq  $\text{yr}^{-1}$ ). Alkalinity is taken up by a population of calcifying  
77 organisms  $C$  (mM eq) growing with rate constant  $k$  ((mM eq) $^{-1}$   $\text{yr}^{-1}$ ) and sedimenting out at rate  $M$  ( $\text{yr}^{-1}$ ).  
78 Altogether, the model equations are:

$$82 \frac{dA}{dt} = I_0 - kAC \quad (1)$$

$$84 \frac{dC}{dt} = kAC - MC \quad (2)$$

85 with  $t$  the time (yr). Since there exists observational evidence of variations in calcifier productivity  
86 correlated with Milankovitch cycles (Beaufort et al., 1997; Herbert, 1997), we include a periodic forcing  
87 term in the calcifier growth parameter  $k$ :

$$90 k = k_0 \left( 1 + \alpha \cos \left( \frac{2\pi t}{T} \right) \right) \quad (3)$$

91 As in Omta et al. (2016) and Shackleton et al. (2023),  $k_0$  is the average value of  $k$ ,  $\alpha$  is the non-  
92 dimensional forcing amplitude, and  $T$  (yr) is the forcing period.

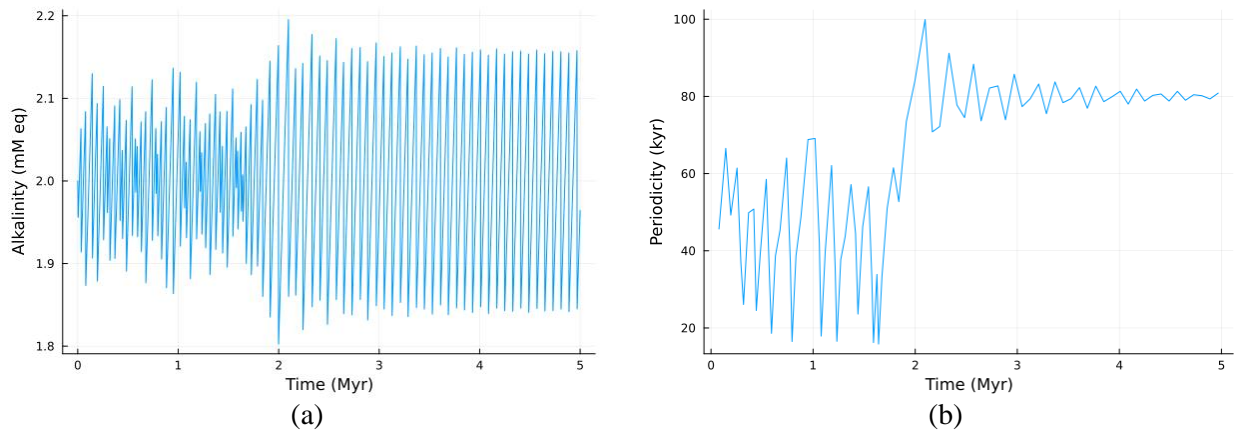
93 Generally speaking, the alkalinity budget is also affected by the seawater carbonate saturation state.  
94 In particular, calcite preservation tends to increase with increasing carbonate ion concentration (Broecker  
95 and Peng, 1982; Archer, 1996). This carbonate compensation feedback was included in the detailed multi-  
96 box version of the calcifier-alkalinity model (Omta et al., 2013). Essentially, carbonate compensation

98 acted as a negative feedback that enhanced the damping of the cycles. If the periodic forcing was  
 99 sufficiently strong to overcome this damping, then the model behavior was very similar to the behavior of  
 100 the model without carbonate compensation (see Fig. 5 in Omta et al., 2013). Here we chose to use the  
 101 simpler, more parsimonious model.

102 Simulations with the C-A model are performed in Julia version 1.11.2. As in Shackleton et al. (2023),  
 103 we use the KenCarp58 solver (Rackauckas and Nie, 2017) with a tolerance of  $10^{-16}$  (code is available on  
 104 GitHub – <https://github.com/AWO-code/VerbitskyOmta>).

### 105 3. Results and Discussion

108 The C-A system (1) – (3) produces sawtooth-shaped cycles in alkalinity, with the alkalinity rising  
 109 slowly and declining steeply. This corresponds to  $\text{CO}_2$  decreasing slowly and increasing rapidly,  
 110 consistent with the ice-core record (Lüthi et al., 2008). In Fig. 1, a simulation with initial conditions  
 111  $A(0) = 2.0 \text{ mM eq}$ ,  $C(0) = 4 * 10^{-5} \text{ mM eq}$ , forcing strength  $\alpha = 0.012$ , forcing period  $T = 40 \text{ kyr}$ , and  
 112 reference values for other parameters (Omta et al., 2016) is shown.



114  
 115 **Figure 1.** C-A system under orbital forcing ( $A(0) = 2.0 \text{ mM eq}$ ,  $C(0) = 4 * 10^{-5} \text{ mM eq}$ ,  $\alpha = 0.012$ ,  $T =$   
 116  $40 \text{ kyr}$ ): (a) alkalinity, (b) dominant period as a function of time

117  
 118 The dominant period initially evolves around the forcing period of 40 kyr, then sharply (MPT-  
 119 like) increases to about 80 kyr (twice the forcing period) and stabilizes at this level. This period shift  
 120 occurs through a different mechanism than in earlier studies using the C-A model, where period shifts  
 121 involved noise (Omta et al., 2016) or a positive feedback (Shackleton et al., 2023) to “kick” the system  
 122 from one dominant period to another one. Here no such kick is imposed: the period shift rather emerges  
 123 as part of the transient dynamics of the system, as it relaxes from its initial towards its asymptotic state.  
 124 For the first  $\sim 1.7 \text{ Myr}$  of the simulation, there appears to be an approximate but not exact frequency lock,  
 125 from which the system has difficulty escaping. Once the system is out of this approximate frequency lock,  
 126 its period increases relatively rapidly until it reaches another multiple of the forcing period where the  
 127 system becomes locked again.

128 In the following, we analyze how the *initial* and *asymptotic* periods may depend on the system  
 129 parameters. In particular, we formulate a scaling law (Section 3.1) that we then investigate in more details  
 130 through simulations (Section 3.2). In Section 3.3 we project the discovered alkalinity dynamics onto the  
 131 glacial rhythmicity.

### 3.1 Scaling law

The C-A system of equations (1) – (3) contains seven governing parameters, including the initial conditions. Both the mean initial and the asymptotic periods have to be functions of these seven parameters. Thus, we can write:

$$P = \varphi(I_0, k_0, \alpha, T, M, A(0), C(0)) \quad (4)$$

with  $P$  the asymptotic period. If we take  $I_0, k_0$  as parameters with independent dimensions, then according to the  $\pi$ -theorem (Buckingham, 1914):

$$\frac{P}{\tau} = \Phi \left[ \alpha, \frac{T}{\tau}, M\tau, \frac{A(0)}{F}, \frac{C(0)}{F} \right] \quad (5)$$

Here  $\tau = (k_0 I_0)^{-1/2}$ ,  $F = \left(\frac{I_0}{k_0}\right)^{1/2}$ .

In this study, we will focus just on two similarity parameters  $\alpha, \frac{A(0)}{F}$  leaving  $\frac{T}{\tau}, M\tau, \frac{C(0)}{F}$  to remain constant:

$$\frac{P}{\tau} = \Phi \left[ \alpha, \frac{A(0)}{F} \right] \quad (6)$$

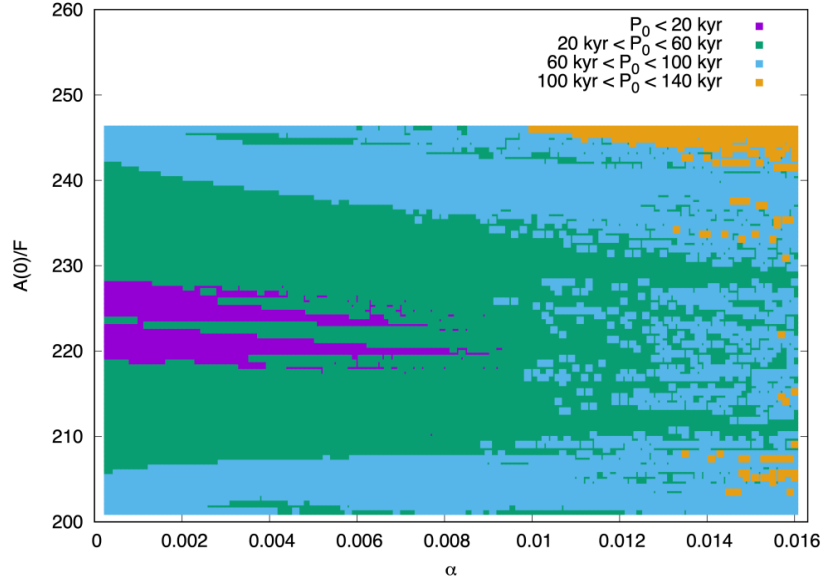
Using similar reasoning, we can write for the initial period  $P_0$ :

$$\frac{P_0}{\tau} = \Psi \left[ \alpha, \frac{A(0)}{F} \right] \quad (7)$$

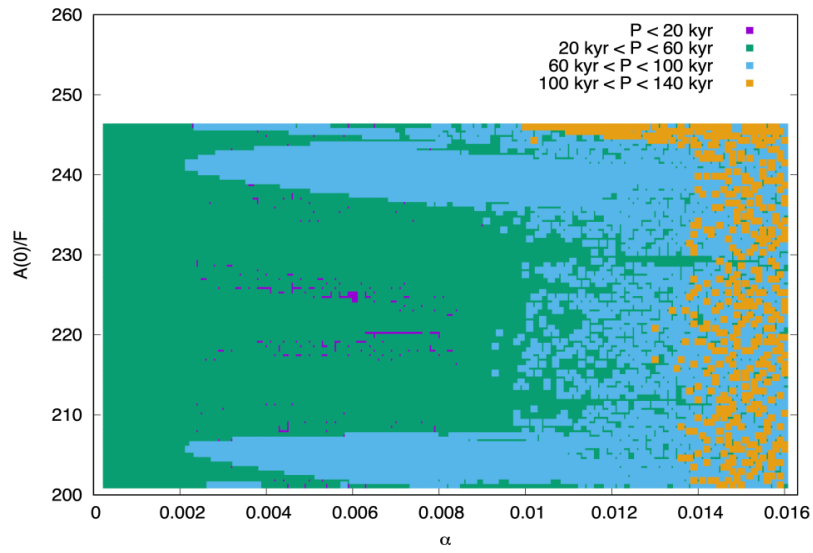
### 3.2 Scaling law simulations

To investigate the scaling laws (6, 7), we perform a suite of 10-Myr simulations in which we vary  $\alpha$  and  $\frac{A(0)}{F}$ . The average periods during the first 1 Myr ( $P_0$ ) and the last 1 Myr ( $P$ ) as a function of  $\alpha$  and  $\frac{A(0)}{F}$  are presented in Figs. 2a and 2b, respectively. The range in  $A(0)$ , which determines the vertical axis range in Fig. 2, was chosen based on the estimated total weathering input of  $\text{CaCO}_3$  (Milliman et al., 1999), which could give rise to alkalinity variations of up to  $\sim 20\%$  on  $\sim 100$ -kyr timescales (Omta et al., 2013). The lower and higher ends of the range are probably a bit less likely than the middle part of the range. There is no obvious constraint on  $\alpha$  (horizontal axis in Fig. 2), which is why we varied that parameter by two orders of magnitude. In total, Fig. 2 encompasses the results of 12,798 simulations.

(a)



(b)



170 **Figure 2.** (a) Initial periods  $P_0$  (average of first 1 Myr of 10-Myr simulations), and (b) asymptotic periods  
171  $P$  (average of last 1 Myr of 10-Myr simulations). Each dot represents one simulation. In total, Fig. 2  
172 encompasses the results of 12,798 simulations. In all simulations,  $T = 40$  kyr and  $C(0) = 4 * 10^{-5}$  mM  
173 eq. Other parameters are kept constant at their reference values (Omta et al., 2016):  $M = 0.1$   $\text{yr}^{-1}$ ,  
174  $k_0 = 0.05$  (mol eq) $^{-1}$   $\text{m}^3$   $\text{yr}^{-1}$ ,  $I_0 = 4 * 10^{-6}$  mol eq  $\text{m}^{-3}$   $\text{yr}^{-1}$ .  
175

176 From Fig. 2, it can be observed that:

177 (a)  $P_0$  and  $P$  depend on  $\alpha$  and  $\frac{A(0)}{F}$  in different manners. Most obviously,  $P_0 < 20$  kyr in a significant  
 178 fraction of the simulations whereas  $P > 20$  kyr in almost every simulation. Furthermore,  $P > 100$  kyr  
 179 occurs in many more simulations than  $P_0 > 100$  kyr. These differences imply that a period shift  
 180 emerges in a significant fraction of the simulations.

181 (b) When  $\alpha \rightarrow 0$ , the asymptotic period  $P$  becomes independent of the initial value  $A(0)$  (Fig. 2b), which  
 182 means that the similarity parameters  $\alpha, \frac{A(0)}{F}$  in the C-A system (1) – (3) collide into one conglomerate  
 183 similarity parameter  $\alpha^x \left[ \frac{A(0)}{F} \right]^y$  (the parameters  $x$  and  $y$  should be determined experimentally). This then  
 184 provides us with the final form of the scaling law for the asymptotic period:

185

186 
$$\frac{P}{\tau} = \Phi \left\{ \alpha^x \left[ \frac{A(0)}{F} \right]^y \right\} \quad (8)$$

187

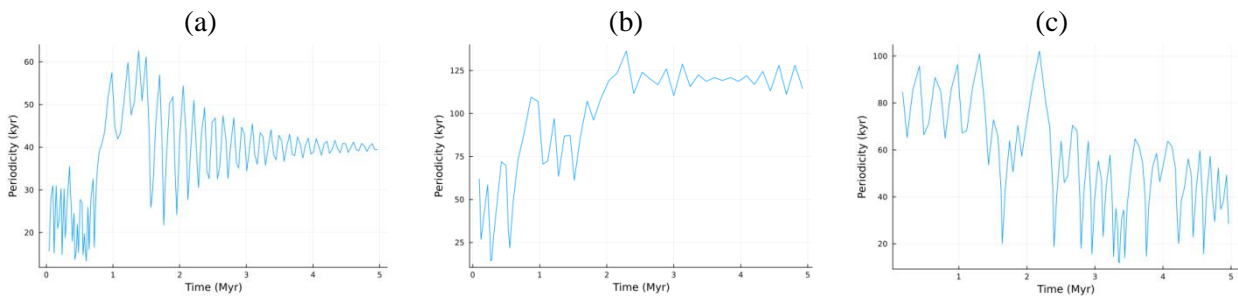
188 The scaling law (8) implies that the *orbital forcing affects the dynamical properties of the C-A physics*  
 189 *enabling the sensitivity of asymptotic periods to initial values.*

190 (c) When  $\alpha$  increases, the sensitivity of the dominant asymptotic period to the initial conditions  $\frac{d(P)}{d(\frac{A(0)}{F})}$   
 191 also increases. Specifically, when  $\alpha < 0.002$ , as we have already noted,  $\frac{P}{\tau}$  is not sensitive to initial  
 192 values. When  $0.002 < \alpha < 0.01$ , it takes  $\Delta \left( \frac{A(0)}{F} \right) \sim 10$  to obtain a different asymptotic period.  
 193 Orbital forcing with  $0.01 < \alpha < 0.014$  reduces the critical value of initial values changes to  
 194  $\Delta \left( \frac{A(0)}{F} \right) \sim 1$ , and finally for  $\alpha > 0.014$  changes as small as  $\Delta \left( \frac{A(0)}{F} \right) \sim 0.1$  lead to different  
 195 asymptotic periods.

196 (d) Depending on  $\alpha^x \left[ \frac{A(0)}{F} \right]^y$ , the periodicity transition could have been not just of the 40 – 80 kyr type (as  
 197 shown in Fig. 1), but also of a 20 – 40, 40 – 120, or even 80 – 40 kyr type (Fig. 3).

198

199



200

201 **Figure 3.** Alkalinity dominant-period transitions of 20 – 40 kyr (a), 40 – 120 kyr (b), and 80 – 40 kyr (c).

202

203 Most of the simulations reach their asymptotic periods within the first 1 Myr. A period shift after  
 204 1 Myr occurs in 3,217 out of the 12,798 simulations (about 25%) represented in Fig. 2, which is a rather  
 205 common occurrence in our view. However, it is impossible to infer from the proxy data how common or  
 206 rare a shift in the dominant period of the glacial-interglacial cycles actually is in the real World, since the  
 207 observed Pleistocene climate is essentially a single time series.

208 Classical phase locking (e.g., Tziperman et al., 2006) requires some kind of dissipation in the  
 209 dynamical system that erases the memory of its initial values. Obviously, this is not the case with the  
 210 dominant-period trajectories we observe in Figs. 1, 2, and 3. At the same time, the asymptotic periods are  
 211 multiples of the forcing period. We therefore suggest calling this phenomenon a *delayed* phase locking.

212                   **3.3 Translating alkalinity dynamics into glacial rhythmicity**

213  
214     To investigate the link between the modelled relaxation process and the climate system, we  
215 applied some alkalinity time series to the Verbitsky et al. (2018) model as additional forcings for the ice  
216 mass balance. This model has been derived from the scaled mass-, momentum-, and heat-conservation  
217 equations of non-Newtonian ice flow combined with an energy-balance model of global climate. In our  
218 experiments, all reference parameters of the Verbitsky et al. (2018) model remain the same, except one  
219 parameter that affects the intensity of positive feedbacks. On its own accord, the Verbitsky et al. (2018)  
220 model can produce a period shift if a positive feedback is sufficiently strong. We now set this positive  
221 feedback weaker to deprive the Verbitsky et al. (2018) model of this ability to produce MPT-like events.

222     In Figure 4a, we show the weak-positive-feedback area-of-glaciation evolution under the imposed  
223 cooling trend without additional alkalinity ( $\text{CO}_2$ ) forcing. This time series does not exhibit MPT-like  
224 periodicity changes. When an additional alkalinity ( $\text{CO}_2$ ) forcing containing a period shift from 41 kyr to  
225 80 kyr is applied, the glaciation-climate system produces a 40-to-100 kyr glacial rhythmicity transition  
226 resembling the LR04 data (Figure 4b vs 4d). This is the case of the direct alkalinity-forced period  
227 transition that could probably be anticipated. Yet, it is quite remarkable and very unintuitive that the  
228 alkalinity forcing may entertain a more subtle interplay with the direct orbital forcing. This becomes  
229 evident in the experiment when we forced the Verbitsky et al. (2018) model with an alkalinity ( $\text{CO}_2$ )  
230 forcing containing periodicity transitions from 20 kyr to 42 kyr. A non-linear interplay of the direct  
231 orbital forcing (i.e., mid-July insolation at  $65^0\text{N}$ , Berger and Loutre, 1991) and of  $\sim$ 40-kyr periods of the  
232 alkalinity forcing may produce glaciation periods of  $\sim$ 100 kyr also consistent with the LR04 data (Figure  
233 4c vs 4d).

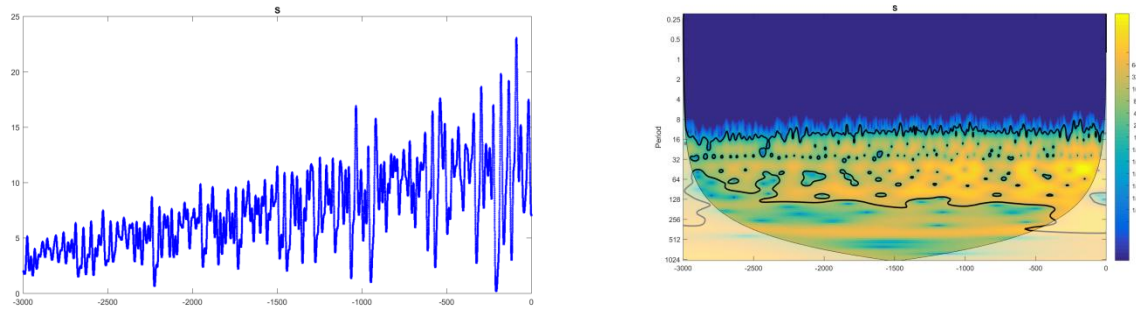
234     In this paper, we do not aspire to precisely reproduce the empirical time series and by doing so to  
235 claim any specific attribution. However, with the above experiments, we demonstrate that the calcifier-  
236 alkalinity dynamics may have a profound effect on the climate system, and what we call an MPT-like  
237 event in terms of the alkalinity periods can be translated into an MPT event in terms of glacial  
238 rhythmicity.

239                   **4. Conclusions**

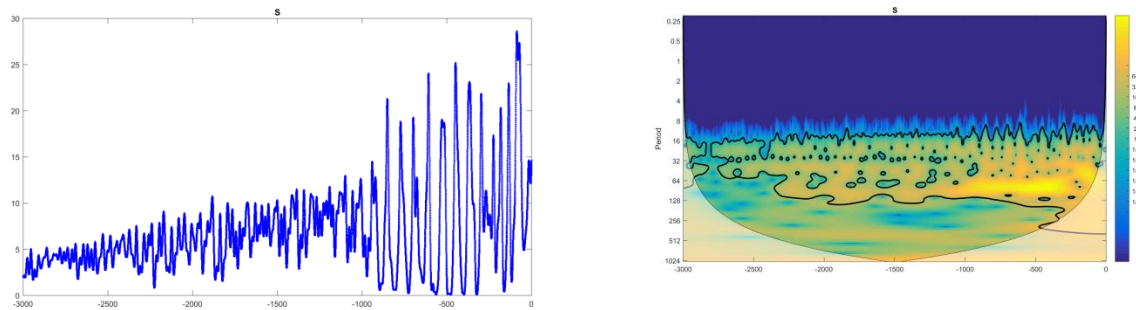
240     The history of climate has been given to us as a single time series. For many years, perhaps  
241 somewhat naively, significant efforts have been applied to reproduce this time-series under a unique  
242 combination of the governing parameters and thus presumably to explain the history. The fundamental  
243 fact that the dominant-period trajectory is governed by a conglomerate similarity parameter

244      $\alpha^x \left[ \frac{A(0)}{F} \right]^y$  (demonstrating a property of incomplete similarity as defined by Barenblatt, 2003) tells us that  
245 the MPT could have been produced under very different combinations of the intensity of orbital forcing  
246 and initial values. Furthermore, the scaling laws (7) and (8), as they are presented in Fig. 2, show that not  
247 only periodicity transitions of the 40 – 80 kyr type (as we observe in the available data), but also of 20 –  
248 40, 40 – 120, or even 80 – 40 kyr types would be possible. Some of these transitions, i.e., 40 – 80, 40 –  
249 120, and, remarkably, 20 – 40 kyr types, produce glaciation MPT events consistently with the data. Most  
250 intriguingly, the conglomerate similarity parameter  $\alpha^x \left[ \frac{A(0)}{F} \right]^y$  implies that such an “intimate” terrestrial  
251 property as the sensitivity of alkalinity-calcination system to initial values manifests itself only under  
252 orbital forcing, and thus *the MPT exhibits a remarkable physical phenomenon of orbitally enabled*  
253 *sensitivity to initial values.*

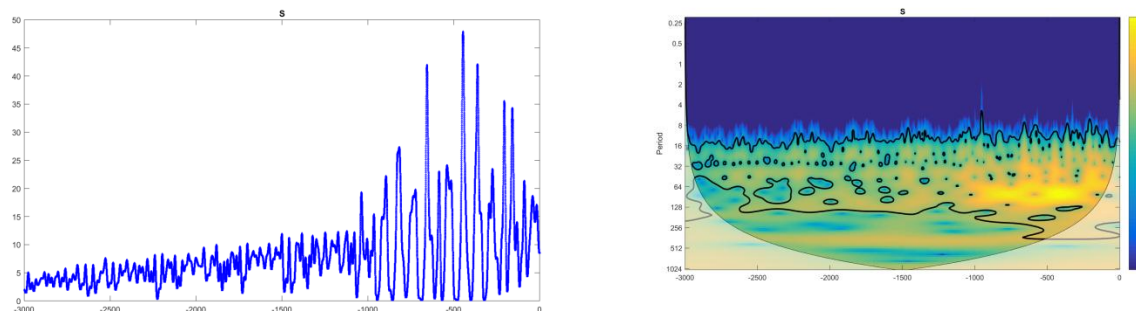
(a)



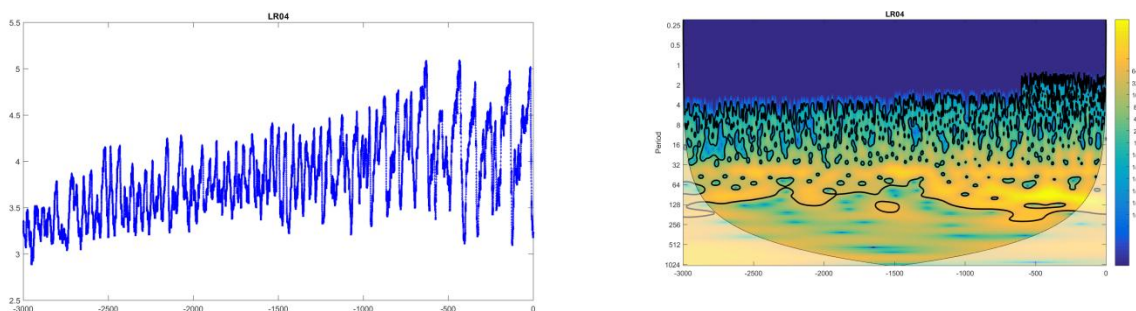
(b)



(c)



(d)



256 **Figure 4.** Ice-climate system (Verbitsky et al., 2018) response to a pure orbital (a) and to a combination of orbital and  
257 alkalinity ( $\text{CO}_2$ ) forcing (b - additional alkalinity ( $\text{CO}_2$ ) forcing contains a periodicity transition from 41 kyr to 80 kyr, c -  
258 additional alkalinity ( $\text{CO}_2$ ) forcing contains a periodicity transition from 20 kyr to 42 kyr) presented as time series and evolutions  
259 of wavelet spectra over 3 Myr for calculated ice-sheet glaciation area  $S$  ( $10^6 \text{ km}^2$ ) (a, b, c) and for the Lisiecki and Raymo (2005)  
260 benthic  $\delta^{18}\text{O}$  record (d). The vertical axis of wavelet spectra is the period (kyr); the horizontal axis is time (kyr before  
261 present). The color scale shows the continuous Morlet wavelet amplitude, the thick line indicates the peaks with 95 % confidence,  
262 and the shaded area indicates the cone of influence for the wavelet transform.

263 **Competing interests:** The authors declare that they have no conflict of interest.

264 **Author contributions:** MYV conceived the research, AWO performed the simulations and discovered  
265 the MPT-like periodicity relaxation, MYV performed the scaling analysis and discovered the orbitally  
266 enabled sensitivity to initial values. The authors jointly wrote and edited the paper.

267 **References**

268 Abe-Ouchi, A., Saito, F., Kawamura, K., Raymo, M. E., Okuno, J., Takahashi, K., and Blatter, H.:  
269 Insolation-driven 100,000-year glacial cycles and hysteresis of ice-sheet volume, *Nature*, 500, 190–193,  
270 <https://doi.org/10.1038/nature12374>, 2013.

271 Archer, D. E.: An atlas of the distribution of calcium carbonate in sediments of the deep sea, *Global*  
272 *Biogeochem. Cycles*, 10, 159–174, 1996.

273 Ashwin, P. and Ditlevsen, P. D.: The middle Pleistocene transition as a generic bifurcation on a slow  
274 manifold, *Clim. Dynam.*, 45, 2683–2695, <https://doi.org/10.1007/s00382-015-2501-9>, 2015.

275 Barenblatt, G. I.: *Scaling*, Cambridge University Press, Cambridge, UK, ISBN 0 521 53394 5, 2003.

276 Beaufort, L., Lancelot, Y., Camberlin, P., Cayre, O., Vincent, E., Bassinot, F., and Labeyrie, L.:  
277 Insolation cycles as a major control of Equatorial Indian Ocean primary production, *Science*, 278, 1451–  
278 1454, 1997.

279 Bintanja, R. and Van de Wal, R. S. W.: North American ice-sheet dynamics and the onset of 100,000-year  
280 glacial cycles, *Nature*, 454, 869–872, <https://doi.org/10.1038/nature07158>, 2008.

281 Broecker, W. S. and Peng, T. H.: *Tracers in the Sea*, Lamont-Doherty Geological Observatory, Palisades,  
282 NY, USA, ISBN 9780961751104, 1982.

283 Buckingham, E.: On physically similar systems; illustrations of the use of dimensional equations, *Phys.*  
284 *Rev.*, 4, 345–376, 1914.

285 Carrillo, J., Mann, M.E., Marinov, I., Christiansen, S.A., Willeit, M. and Ganopolski, A.: Sensitivity of  
286 simulations of Plio–Pleistocene climate with the CLIMBER-2 Earth System Model to details of the global  
287 carbon cycle. *Proceedings of the National Academy of Sciences*, 122(23), p.e2427236122, 2025.

288 Clark, P. U. and Pollard, D.: Origin of the middle Pleistocene transition by ice sheet erosion of regolith,  
289 *Paleoceanography*, 13, 1–9, 1998.

290 Crucifix, M.: Why could ice ages be unpredictable?, *Clim. Past*, 9, 2253–2267,  
291 <https://doi.org/10.5194/cp-9-2253-2013>, 2013.

292 Herbert, T.: A long marine history of carbon cycle modulation by orbital-climatic changes, *Proc. Natl.*  
293 *Acad. Sci.*, 94, 8362–8369, 1997.

294 Lisiecki, L. E. and Raymo, M. E.: A Pliocene-Pleistocene stack of 57 globally distributed benthic  $\delta^{18}\text{O}$   
295 records, *Paleoceanography*, 20, PA1003, <https://doi.org/10.1029/2004PA001071>, 2005.

296 Lüthi, D., Le Floch, M., Bereiter, B., Blunier, T., Barnola, J. M., Siegenthaler, U., Raynaud, D., Jouzel, J.,  
297 Fischer, H., Kawamura, K., and Stocker, T.F.: High-resolution carbon dioxide concentration record  
298 650,000-800,000 years before present, *Nature*, 453, 379–382, <https://doi.org/10.1038/nature06949>, 2008.

299 Ma, X., Yang, M., Sun, Y., Dang, H., Ma, W., Tian, J., Jiang, Q., Liu, L., Jin, X. and Jin, Z.: The  
300 potential role of insolation in the long-term climate evolution since the early Pleistocene. *Global and*  
301 *Planetary Change*, 240, 104526, 2024.

302 Milliman, J. D., Troy, P. J., Balch, W. M., Adams, A. K., Li, Y. H., and Mackenzie, F. T.: Biologically  
303 mediated dissolution of calcium carbonate above the chemical lysocline?, *Deep Sea Res. Part I*, 46, 1653–  
304 1669, 1999.

305 Mitsui, T. and Aihara, K.: Dynamics between order and chaos in conceptual models of glacial cycles,  
306 *Clim. Dynam.*, 42, 3087–3099, 2014.

307 Nyman, K. H. M., and Ditlevsen, P. D.: The Middle Pleistocene Transition by frequency locking and  
308 slow ramping of internal period, *Clim. Dynam.*, 53, 3023–3038, <https://doi.org/10.1007/s00382-019-04679-3>, 2019.

310 Omta, A.W., Van Voorn, G.A.K., Rickaby, R.E.M., Follows, M.J.: On the potential role of marine  
311 calcifiers in glacial–interglacial dynamics, *Global Biogeochem. Cycles*, 27, 692–704,  
312 <https://doi.org/10.1002/gbc.20060>, 2013.

313 Omta, A.W., Kooi, B. W., Van Voorn, G.A.K., Rickaby, R.E.M., Follows, M.J.: Inherent characteristics  
314 of sawtooth cycles can explain different glacial periodicities, *Clim. Dynam.*, 46, 557–569,  
315 <https://doi.org/10.1007/s00382-015-2598-x>, 2016.

316 Paillard, D.: Quaternary glaciations: from observations to theories, *Quaternary Sci. Rev.*, 107, 11–24,  
317 <https://doi.org/10.1016/j.quascirev.2014.10.002>, 2015.

318 Peacock, S., Lane, E., and Restrepo, J. M.: A possible sequence of events for the generalized glacial–  
319 interglacial cycle, *Global Biogeochem. Cycles*, 20, GB2010, <https://doi.org/10.1029/2005GB002448>,  
320 2006.

321 Pérez-Montero, S., Alvarez-Solas, J., Swierczek-Jereczek, J., Moreno-Parada, D., Robinson, A., and  
322 Montoya, M.: Understanding the Mid-Pleistocene transition with a simple physical model, *EGU*sphere  
323 [preprint], <https://doi.org/10.5194/egusphere-2025-2467>, 2025.

324 Rackauckas, C. and Nie, Q.: Differential equations.jl - A performant and feature-rich ecosystem for  
325 solving differential equations in Julia, *J. Open Res. Softw.*, 5, 15, <https://doi.org/10.5334/jors.151>, 2017.

326 Raymo, M. E., Lisiecki, L. E., and Nisancioglu, K. H.: Plio-Pleistocene Ice Volume, Antarctic Climate,  
327 and the Global  $\delta^{18}\text{O}$  Record, *Science*, 313, 492–495, <https://doi.org/10.1126/science.1123296>, 2006.

328 Rial, J. A., Oh, J., and Reischmann, E.: Synchronization of the climate system to eccentricity forcing and  
329 the 100,000-year problem, *Nature Geosci.*, 6, 289–293, <https://doi.org/10.1038/ngeo1756>, 2013.

330 Riechers, K., Mitsui, T., Boers, N., and Ghil, M.: Orbital insolation variations, intrinsic climate  
331 variability, and Quaternary glaciations, *Clim. Past*, 18, 863–893, <https://doi.org/10.5194/cp-18-863-2022>,  
332 2022.

333 Saltzman, B. and Verbitsky, M. Y.: Multiple instabilities and modes of glacial rhythmicity in the Plio-  
334 Pleistocene: a general theory of late Cenozoic climatic change, *Clim. Dynam.*, 9, 1–15, 1993.

335 Scherrenberg, M. D. W., Berends, C. J., and Van de Wal, R. S. W.: CO<sub>2</sub> and summer insolation as drivers  
336 for the Mid-Pleistocene Transition, *Clim. Past*, 21, 1061–1077, <https://doi.org/10.5194/cp-21-1061-2025>,  
337 2025.

338 Shackleton, J. D., Follows, M. J., Thomas P. J., and Omta, A. W.: The Mid-Pleistocene Transition: a  
339 delayed response to an increasing positive feedback? *Clim. Dynam.*, 60, 4083–4098,  
340 <https://doi.org/10.1007/s00382-022-06544-2>, 2023.

341 Tzedakis, P. C., Crucifix, M., Mitsui, T., and Wolff, E. W.: A simple rule to determine which insolation  
342 cycles lead to interglacials, *Nature*, 542, 427–432, <https://doi.org/10.1038/nature21364>, 2017.

343 Tziperman, E., Raymo, M. E., Huybers, P., and Wunsch, C.: Consequences of pacing the Pleistocene  
344 100 kyr ice ages by nonlinear phase locking to Milankovitch forcing, *Paleoceanography*, 21, PA4206,  
345 <https://doi.org/10.1029/2005PA001241>, 2006.

346 Verbitsky, M. Y. and Crucifix, M.: ESD Ideas: The Peclet number is a cornerstone of the orbital and  
347 millennial Pleistocene variability, *Earth Syst. Dynam.*, 12, 63–67, <https://doi.org/10.5194/esd-12-63-2021>, 2021.

349 Verbitsky, M. Y. and Volobuev, D.: Milankovitch Theory “as an Initial Value Problem”, *EGU*sphere  
350 [preprint], <https://doi.org/10.5194/egusphere-2024-1255>, 2024.

351 Verbitsky, M. Y., Crucifix, M., and Volobuev, D. M.: A theory of Pleistocene glacial rhythmicity, *Earth*  
352 *Syst. Dynam.*, 9, 1025–1043, <https://doi.org/10.5194/esd-9-1025-2018>, 2018.

353 Willeit, M., Ganopolski, A., Calov, A., and Brovkin, V.: Mid-Pleistocene transition in glacial cycles  
354 explained by declining CO<sub>2</sub> and regolith removal, *Science Advances* 5, 4,  
355 <https://www.science.org/doi/10.1126/sciadv.aav7337>, 2019.

356

357 Williams, R.G. and Follows, M.J.: Ocean dynamics and the carbon cycle, Cambridge University Press,  
358 Cambridge, UK, ISBN 9780521843690, 2011.

359

360 Zeebe, R. E. and Wolf-Gladrow, D.A.: CO<sub>2</sub> in seawater: Equilibrium, kinetics, isotopes, Elsevier,  
361 Amsterdam, Netherlands, ISBN 9780444509468, 2001.